# Infrared absorption of trans-1-chloromethylallyl and trans-1-methylallyl radicals produced in photochemical reactions of trans-1,3-butadiene and C2 in solid para-hydrogen

Mohammed Bahou, Jen-Yu Wu, Keiichi Tanaka, and Yuan-Pern Lee

Citation: The Journal of Chemical Physics **137**, 084310 (2012); doi: 10.1063/1.4745075
View online: http://dx.doi.org/10.1063/1.4745075
View Table of Contents: http://scitation.aip.org/content/aip/journal/jcp/137/8?ver=pdfcov
Published by the AIP Publishing

# Infrared absorption of *trans*-1-chloromethylallyl and *trans*-1-methylallyl radicals produced in photochemical reactions of *trans*-1,3-butadiene and $C\ell_2$ in solid *para*-hydrogen

Mohammed Bahou,[1] Jen-Yu Wu,[1] Keiichi Tanaka,[1] and Yuan-Pern Lee[1,2,a)]
[1]*Department of Applied Chemistry and Institute of Molecular Science, National Chiao Tung University, 1001 Ta-Hsueh Rd., Hsinchu 30010, Taiwan*
[2]*Institute of Atomic and Molecular Sciences, Academia Sinica, Taipei 10617, Taiwan*

(Received 10 May 2012; accepted 26 July 2012; published online 28 August 2012)

The reactions of chlorine and hydrogen atoms with *trans*-1,3-butadiene in solid *para*-hydrogen (*p*-$H_2$) were investigated with infrared (IR) absorption spectra. When a *p*-$H_2$ matrix containing $C\ell_2$ and *trans*-1,3-butadiene was irradiated with ultraviolet light at 365 nm, intense lines at 650.3, 809.0, 962.2, 1240.6 $cm^{-1}$, and several weaker ones due to the *trans*-1-chloromethylallyl radical, $\bullet(CH_2CHCH)CH_2C\ell$, appeared. Observed wavenumbers and relative intensities agree with the anharmonic vibrational wavenumbers and IR intensities predicted with the B3PW91/6-311++g(2*d*, 2*p*) method. That the $C\ell$ atom adds primarily to the terminal carbon atom of *trans*-1,3-butadiene is in agreement with the path of minimum energy predicted theoretically, but in contrast to the reaction of $C\ell$ + propene in solid *p*-$H_2$ [J. Amicangelo and Y.-P. Lee, J. Phys. Chem. Lett. **1**, 2956 (2010)] in which the addition of $C\ell$ to the central C atom is favored, likely through steric effects in a *p*-$H_2$ matrix. A second set of lines, intense at 781.6, 957.9, 1433.6, 2968.8, 3023.5, 3107.3 $cm^{-1}$, were observed when the UV-irradiated $C\ell_2$/*trans*-1,3-butadiene/*p*-$H_2$ matrix was further irradiated with IR light from a SiC source. These lines are assigned to the *trans*-1-methylallyl radical, $\bullet(CH_2CHCH)CH_3$, produced from reaction of 1,3-butadiene with a H atom resulted from the reaction of $C\ell$ atoms with solid *p*-$H_2$ exposed to IR radiation. © *2012 American Institute of Physics*. [http://dx.doi.org/10.1063/1.4745075]

## I. INTRODUCTION

Unsaturated hydrocarbon radicals are important intermediates in combustion reactions; their reaction kinetics have been investigated extensively to understand combustion processes.[1–4] The dissociation and mechanism of isomerization of $C_3H_5$ and $C_4H_7$ radicals, for example, have been studied both experimentally[5–12] and theoretically[13–17] to understand the branching ratios among various dissociation channels as a function of excitation energy. The reactions of alkenes ($C_nH_{2n}$) with atomic chlorine ($C\ell$) play important roles in the chemistry of the polar troposphere;[18–20] these reactions have also been studied extensively with theory.[21–23] The two most significant initial processes of $C\ell + C_nH_{2n}$ reactions are the addition of a $C\ell$ atom to form a chloroalkyl radical ($\bullet C_nH_{2n}C\ell$) and the abstraction of a H atom by the $C\ell$ atom to form an alkyl radical ($\bullet C_nH_{2n-1}$) and $HC\ell$.[24] In most cases, the infrared (IR) spectra of the chloroalkyl radical remain unidentified because of the instability of these species and the final products are generally the dichloroalkanes when molecular chlorine reacts with alkenes in a solution or in the gaseous phase.[25,26]

Photochemical reactions in solid *para*-hydrogen (*p*-$H_2$) at low temperature have generated considerable interest in recent years.[27,28] The *p*-$H_2$ matrix is considered to be a quantum solid as the amplitude of the zero-point lattice vibrations is a large fraction of the lattice spacing.[29] One unique feature of the *p*-$H_2$ matrix is that it is *softer* than noble-gas matrices, such as Ar and Ne, such that the matrix cage effect is diminished. A recent study of matrix-isolated water dimers indicated that, for a given monomer concentration, the dimer concentration is significantly higher in solid Ne (or Ar) than in solid *p*-$H_2$.[30] However, because the photofragments can diffuse in solid *p*-$H_2$, formation of complexes prior to photolysis might not be the critical criterion for bimolecular reaction to take place in a *p*-$H_2$ matrix; the more critical property is the diminished cage effect so that the fragments can escape from the original cage to become isolated or react with other guest molecules. Furthermore, one can always perform moderate annealing after deposition to enhance the formation of complexes. As a consequence, photoproducts such as $C\ell$ atom and $CH_3$ radical produced on ultraviolet (UV) irradiation of $C\ell_2$ (Ref. 31) and $CH_3I$,[32–34] respectively, become excellent sources for studying bimolecular reactions in solid *p*-$H_2$. We have employed this method to investigate the reactions of $C\ell$ or $CH_3$ with several small molecules in solid *p*-$H_2$. For instance, the reaction $C\ell + CS_2$ in *p*-$H_2$ produced $C\ell SCS$, $C\ell CS$, and $C\ell SC$,[35] $C\ell$ + propene ($C_3H_6$ or $CH_2{=}CHCH_3$) produced the 2-chloropropyl radical ($\bullet CH_2CHC\ell CH_3$),[36] and $CH_3 + SO_2$ produced $CH_3SO_2$.[34]

In the reaction $C\ell + C_3H_6$ in solid *p*-$H_2$, we observed IR lines ascribable to only the 2-chloropropyl radical, not the 1-chloropropyl radical, $\bullet CH(CH_2C\ell)CH_3$. This result is in contrast to the reported gaseous experiments in which

a)Author to whom correspondence should be addressed. Electronic mail: yplee@mail.nctu.edu.tw.

 

formation of 1-chloropropyl is favored over 2-chloropropyl at least six fold.[37] High-level quantum-chemical computations on the reaction $C\ell + C_3H_6$, however, predicted that the addition of the $C\ell$ atom to either carbon atom involving the double bond is barrierless, and the formation of 1-chloropropyl is energetically favored by less than 1 kJ $mol^{-1}$ over that of 2-chloropropyl, indicating little preference for the addition of $C\ell$ to the terminal versus the central carbon atom.[23] A proposed explanation of this unique selectivity observed in the reaction of $C\ell + C_3H_6$ in solid *p*-$H_2$ involves the steric effects within the solid *p*-$H_2$ matrix that cause the reacting $C\ell$ atom to be guided to the central C atom of $C_3H_6$ embedded in a single substitutional matrix site.[36]

In this work, we extend the study of $C\ell + C_3H_6$ to $C\ell$ + *trans*-1,3-butadiene ($H_2C{=}CH{-}CH{=}CH_2$, hereafter indicated as $C_4H_6$), which has two double bonds and a molecular size larger than $C_3H_6$. We observed absorption lines ascribable to the *trans*-1-chloromethylallyl radical, $\bullet(CH_2CHCH)CH_2C\ell$, indicating that $C\ell$ was added to the terminal carbon of $C_4H_6$. When the UV-irradiated matrix was further irradiated with IR light, we observed lines in another set ascribable to the *trans*-1-methylallyl radical, $\bullet(CH_2CHCH)CH_3$, indicating the addition of H atom also to the terminal carbon of $C_4H_6$.

## II. EXPERIMENTS

The experimental setup has been described previously.[35,36,38] In these experiments, a flow of a mixture of *trans*-1,3-butadiene seeded in *p*-$H_2$ at a rate of 0.010 mol $h^{-1}$ was co-deposited for 3−4 h with a small flow of pure $C\ell_2$ onto a gold-plated copper flat, maintained at 3.3 K with a closed-cycle helium refrigerator (Janis, SHI-415). Typically, the mixing ratio of $C_4H_6/C\ell_2/p$-$H_2$ thus deposited was estimated to be approximately 1.0/1.5/1500.

Infrared absorption spectra were recorded with a Fourier-transform infrared (FTIR) spectrometer (Bomem, DA8) equipped with a KBr beam splitter and a HgCdTe detector cooled to 77 K to cover the spectral range of 500–5000 $cm^{-1}$. The gold-plated copper flat, on which the mixture of $C_4H_6/C\ell_2/p$-$H_2$ was deposited, served also as a mirror to reflect the incident IR light to the detector. Typically, 600 scans were coadded at each stage of experiment with resolution 0.25 $cm^{-1}$.

After deposition, the matrix was irradiated with light at 365 ± 10 nm from a light-emitting diode (Honle UV Technology, 375 mW) for several hours to produce $C\ell$ atoms for reactions with $C_4H_6$. In some experiments, after deposition, the matrix was annealed at 4.3 K for 1 h to enhance the formation of the molecular complex $C\ell_2$-$C_4H_6$. Because excitation of a *p*-$H_2$ matrix containing $C\ell$ atoms with IR light above 4000 $cm^{-1}$ induces the reaction $C\ell + H_2 \rightarrow H + HC\ell$,[39,40] we placed a 2.4-$\mu$m cutoff filter (Andover) before the IR-beam entrance window of the matrix system during spectral data acquisition so as to avoid the reaction of $C\ell$ atoms with *p*-$H_2$. In experiments on $H + C_4H_6$, to promote the formation of H atoms from the reaction of $C\ell$ atoms with *p*-$H_2$ matrix, we removed the 2.4-$\mu$m filter and utilized the IR source of the FTIR spectrometer to excite either the UV-irradiated matrix or the matrix concurrently with the 365-nm light. To distinguish various groups of IR lines observed upon photolysis, secondary photolysis was performed with a low-pressure Hg lamp (Pen-Ray lamp, UVP) with a bandpass filter (254 ± 10 nm, ESCO Products).

$C_4H_6$ (99.5%, Scientific Gas Products) and $C\ell_2$ (99.9%, Air Products) were used without further purification. The *p*-$H_2$ was prepared by catalytic conversion at low temperature. Normal $H_2$ gas (99.9999%, Scott Specialty Gases) passed through a trap at 77 K and a copper coil filled with hydrated iron (III) oxide (30−50 mesh, Sigma-Aldrich) that was cooled with a helium refrigerator (Advanced Research Systems, DE204AF). At the temperature of the catalyst, typically 11–13 K, the concentration of *o*-$H_2$ is estimated to be less than 100 ppm.

## III. QUANTUM-CHEMICAL CALCULATIONS

Density-functional theory (DFT) calculations with the B3PW91 hybrid functional[41–43] and the 6-311++g(2*d*, 2*p*) basis set[44] were performed to predict equilibrium geometries and vibrational wavenumbers of possible products of the reactions $C\ell + C_4H_6$ and $H + C_4H_6$. The PW91 functional has shown advantages in the prediction of binding energies and geometries of weakly bound complexes,[45–47] and B3PW91 is one of the family of Becke three parameter hybrid functionals with non-local correlation provided by the PW91 functional.[41] Analytic first and second derivatives were employed for geometry optimization and vibrational wavenumbers at each stationary point. The anharmonic effects were calculated with a second-order perturbation approach using effective finite-difference evaluation of the third and semi-diagonal fourth derivatives. The GAUSSIAN 09 program was used for the calculations.[48] Unless specified, the calculations were performed for the isotope $^{35}C\ell$.

### A. $C_4H_6$ and the $C\ell_2$-$C_4H_6$ complex

The geometries of *trans*-1,3-butadiene $C_4H_6$ and the $C\ell_2$-$C_4H_6$ complex optimized with the B3PW91/6-311++g(2*d*, 2*p*) calculations are shown in Fig. S1 of the supplementary material;[49] the atomic numbering is indicated in the figure and the $C\ell_2$ is attaching to the C4 and C3 atoms. $C_4H_6$ has a planar C=C–C=C geometry; the calculated C=C and C–C bond lengths (1.334 and 1.451 Å) agree with the experimental values (1.338 and 1.454 Å).[50] In $C\ell_2$-$C_4H_6$, $C\ell_2$ is attached to one C=C bond of $C_4H_6$ nearly perpendicular to the molecular plane of $C_4H_6$. The distance between $C\ell$ and the terminal carbon ($C\ell$–C4, 2.741 Å) is smaller than that between $C\ell$ and the inner carbon ($C\ell$–C3, 2.970 Å); the angle ∠C4C$\ell$C$\ell$ is 168.4°.

Harmonic and anharmonic vibrational wavenumbers of $C_4H_6$ were calculated with the B3PW91/6-311++g(2*d*, 2*p*) method. Vibrational modes $\nu_{11}$ ($CH_2$ wag, $a_u$, 925 $cm^{-1}$), $\nu_{10}$ (out-of-plane CH bend, $a_u$, 1030 $cm^{-1}$), and $\nu_{20}$ (C=C stretch, $b_u$, 1616 $cm^{-1}$) were predicted to have IR intensities greater than 20 km $mol^{-1}$; the listed values are anharmonic vibrational wavenumbers.

Harmonic and anharmonic vibrational wavenumbers and IR intensities of $C\ell_2$-$C_4H_6$ predicted with the

TABLE I. Comparison of vibrational wavenumbers and IR intensities of the $C\ell_2$-*trans*-1,3-butadiene ($C\ell_2$-$C_4H_6$) complex derived from experiments and calculations using the B3PW91/6-311++g(2*d*, 2*p*) method.

| Mode[a] | Sym.[a] | Description[b] | Harmonic ($cm^{-1}$) | Anharmonic ($cm^{-1}$) | Anharmonic Shift[c] | *p*-$H_2$ matrix ($cm^{-1}$) | *p*-$H_2$ matrix Shift[c] |
|---|---|---|---|---|---|---|---|
| $\nu_{17}$ | $b_u$ | *a*-$\nu_{CH2}$ | 3250 (1)[d] | 3105 | 7.2 | 3098.2 (1)[e] | ~0 |
| $\nu_1$ | $a_g$ | *a*-$\nu_{CH2}$ | 3242 (4) | 3097 | − 0.2 | [f] | |
| $\nu_{18}$ | $b_u$ | $\nu_{CH}$ | 3163 (4) | 3025 | 7.6 | [f] | |
| $\nu_2$ | $a_g$ | *s*-$\nu_{CH2}$ + $\nu_{CH}$ | 3157 (3) | 3016 | 5.4 | [f] | |
| $\nu_{19}$ | $b_u$ | *s*-$\nu_{CH2}$ | 3152 (2) | 2992 | 5.3 | [f] | |
| $\nu_3$ | $a_g$ | $\nu_{CH}$ + *s*-$\nu_{CH2}$ | 3148 (1) | 3006 | 7.3 | [f] | |
| $\nu_4$ | $a_g$ | $\nu_{C=C}$ | 1694 (20) | 1649 | − 8.7 | 1640.4 (7) | Activated[g] |
| $\nu_{20}$ | $b_u$ | $\nu_{C=C}$ | 1635 (46) | 1602 | − 14.5 | 1591.8 (56) | −3.3 |
| $\nu_5$ | $a_g$ | $\delta_S$ CH2 | 1474 (1) | 1440 | 2.3 | | |
| $\nu_{21}$ | $b_u$ | $\delta_S$ CH2 | 1412 (5) | 1383 | 0.3 | 1378.9 (3) | ~0 |
| $\nu_{22}$ | $b_u$ | $\delta_{CCH}$ | 1320 (1) | 1294 | 3.9 | | 1.2 |
| $\nu_6$ | $a_g$ | $\delta_{CCH}$ | 1312 (5) | 1278 | − 22.5 | 1281.8 (1) | Activated |
| $\nu_7$ | $a_g$ | $\nu_{C–C}$ | 1233 (1) | 1206 | − 0.6 | | |
| $\nu_{10}$ | $a_u$ | oop $\delta_{CH}$ | 1047 (23) | 1025 | − 4.9 | 1016.2 (26) | 1.0 |
| $\nu_{23}$ | $b_u$ | $\rho_{CH2}$ | 1003 (1) | 990 | 0.4 | 987.8 (1) | ~0 |
| $\nu_{14}$ | $b_g$ | oop $\delta_{CH}$ | 995 (0) | 977 | − 4.1 | | |
| $\nu_{11}$ | $a_u$ | $\omega_{CH2}$ | 954 (62) | 940 | 15.1 | 914.5 (100) | 5.6 |
| $\nu_{15}$ | $b_g$ | $\omega_{CH2}$ | 950 (20) | 939 | 14.2 | 918.9 (40) | Activated |
| $\nu_8$ | $a_g$ | $\rho_{CH2}$ | 905 (1) | 891 | 2 | | |
| $\nu_{16}$ | $b_g$ | $t_{CH2}$ | 784 (1) | 773 | 2.7 | 755.3 (1) | Activated |
| $\nu_{12}$ | $a_u$ | $t_{CH2}$ | 562 (7) | 549 | 12.7 | 534.2 (8) | 5.6 |
| $\nu_9$ | $a_g$ | $\delta_{CCC}$ | 514 (0) | 514 | − 0.7 | | |
| | | $\nu$ C$\ell$–C$\ell$ (35-35) | 455 (100) | 460 | | 524.4 (22) | Activated |
| | | $\nu$ C$\ell$–C$\ell$ (35/37) | | | | 517.3/519.0 (15) | Activated |
| $\nu_{24}$ | $b_u$ | $\delta_{CCC}$ | 292 (2) | 299 | 3.4 | | |
| $\nu_{13}$[g] | $a_u$ | $\tau_{C–C}$ | 197 (2)[h] | 191[h] | 21.1 | | |

[a]Mode numbers and symmetry are listed according to those of $C_4H_6$ for comparison.
[b]Approximate mode description. $\nu$: stretch, $\delta$: bend or deformation, $\delta_S$: scissor, $\omega$: wag, $\rho$: rock, $\tau$: torsion, *t*: twist, *a*: antisymmetric, *s*: symmetric, oop: out-of-plane.
[c]Shift (in $cm^{-1}$) relative to the corresponding features of *trans*-1,3-butadiene.
[d]Numbers in parentheses are IR intensities in km $mol^{-1}$ normalized to the most intense line ($\nu_{C\ell–C\ell}$, intensity 84 km $mol^{-1}$).
[e]Numbers in parentheses are integrated intensities normalized to the most intense one.
[f]Observed lines at 3052.2, 3029.9, 3006.7, 2990.5, and 2980.4 $cm^{-1}$, but definitive mode assignments are uncertain.
[g]The IR inactive modes of $C_4H_6$ are activated upon complex formation.
[h]Additional modes are predicted to have harmonic (IR intensity)/anharmonic vibrational wavenumbers: 145 (3)/126, 117 (12)/107, 98 (7)/89, 87 (0)/72, and 40 (0)/31 $cm^{-1}$.

B3PW91/6-311++g(2*d*, 2*p*) method are listed in Table I; for comparison, the mode numbers and symmetry corresponding to $C_4H_6$ are listed. The predicted shifts of anharmonic vibrational wavenumbers from $C_4H_6$ are also listed. Wavenumbers of lines of the $C\ell_2$-$C_4H_6$ complex corresponding to those of the intense lines of $C_4H_6$, $\nu_{11}$ (940 $cm^{-1}$), $\nu_{10}$ (1025 $cm^{-1}$), and $\nu_{20}$ (1602 $cm^{-1}$), shift slightly; the former is blueshifted, whereas the latter two are redshifted. Some IR inactive modes of $C_4H_6$ with $a_g$ or $b_g$ symmetry become activated through the interaction with $C\ell_2$; two most intense ones are $\nu_{15}$ (939 $cm^{-1}$) and $\nu_4$ (1649 $cm^{-1}$). The C$\ell$–C$\ell$ stretching mode (460 $cm^{-1}$) is activated in $C\ell_2$-$C_4H_6$ and is predicted to have the largest intensity (84 km $mol^{-1}$).

### B. Reaction products of C$\ell$ + $C_4H_6$

The optimized geometries of three possible products of the reaction C$\ell$ + $C_4H_6$ are presented in Fig. 1; the atomic numbering of each species is indicated. The *trans*-1-chloromethylallyl radical, •($CH_2CHCH$)$CH_2C\ell$, has a planar CCCC structure with the unpaired electron delocalized over C1, C2, and C3. Two conformers are stable: conformer (**1a**) with the C$\ell$ atom located nearly perpendicular to the allyl molecular plane with a dihedral angle of $\phi$H4CCC$\ell$ = 70.5° is most stable, and conformer (**1b**) with the C$\ell$ atom in the allyl molecular plane has energy ~8 kJ $mol^{-1}$ above (**1a**). The lengths of bonds C1–C2 and C2–C3 in (**1a**), 1.375 and 1.385 Å, respectively, are slightly greater than the predicted C=C bond length of 1.334 Å in $C_4H_6$.

In contrast, the unpaired electron of the 2-chloro-3-buten-1-yl radical, •$CH_2CHC\ell CH{=}CH_2$, is localized on the terminal carbon C4. Two conformers are stable: the more stable conformer (**2a**) has the chlorine atom located off the C1C2C3 plane with an angle of ∠C2C3C$\ell$ = 107.3° and the C1=C2 and C2–C3 bond lengths of 1.327 and 1.485 Å, respectively. Its energy is ~65 kJ $mol^{-1}$ above *trans*-1-chloromethylallyl (**1a**), rationalized as due to the lack of delocalization of the unpaired electron. The conformer (**2b**) with the chlorine atom in the C1C2C3 molecular plane has energy ~7 kJ $mol^{-1}$ greater than that of (**2a**).

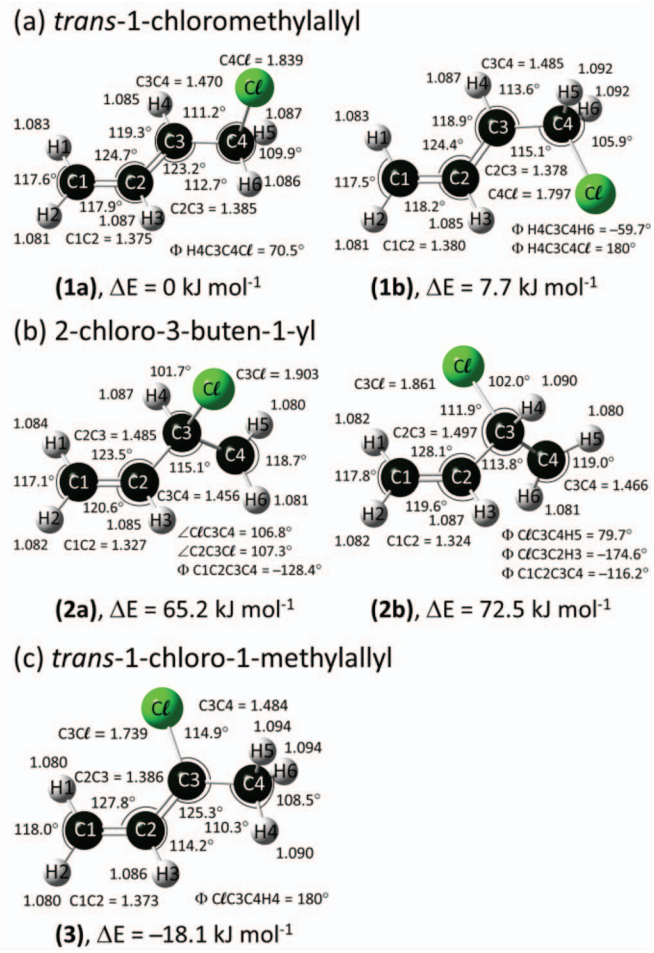


FIG. 1. Geometries of (a) *trans*-1-chloromethylallyl ((**1a**) and (**1b**)), (b) 2-chloro-3-buten-1-yl ((**2a**) and (**2b**)), and (c) *trans*-1-chloro-1-methylallyl (**3**) predicted with the B3PW91/6-311++g(2*d*, 2*p*) method. Bond distances are in Å, and angles in degrees.

The $\bullet(CH_2CHCC\ell)CH_3$ (*trans*-1-chloro-1-methylallyl) radical has one stable conformer (**3**), with the in-plane H atom of the methyl moiety *trans* to the C$\ell$ atom. It is more stable than *trans*-1-chloromethylallyl (**1a**) by 18 kJ mol$^{-1}$. This radical has the unpaired electron delocalized over C1C2C3 with the C1–C2 and C2–C3 bond lengths of 1.373 and 1.386 Å, respectively.

The predicted harmonic and anharmonic vibrational wavenumbers and IR intensities for conformers (**1a**) and (**1b**) of the *trans*-1-chloromethylallyl radical are listed in Table II; the mode order and approximate mode descriptions follow those of (**1a**). Modes $\nu_{21}$ (CC$\ell$ stretch, 610 cm$^{-1}$), $\nu_{19}$ (C1H$_2$ wag, 824 cm$^{-1}$), $\nu_{16}$ (out-of-plane CH bend, 966 cm$^{-1}$), and $\nu_{12}$ (C4H$_2$ wag, 1228 cm$^{-1}$) for (**1a**) have IR intensities greater than 20 km mol$^{-1}$ and those of $\nu_{21}$ (697 cm$^{-1}$), $\nu_{19}$ (796 cm$^{-1}$), $\nu_{16}$ (982 cm$^{-1}$), $\nu_{12}$ (1266 cm$^{-1}$), $\nu_{11}$ (sym. C1C2C3 stretch, 1252 cm$^{-1}$), and $\nu_6$ (C4H$_2$ sym. stretch, 2947 cm$^{-1}$) for (**1b**) have IR intensities greater than 15 km mol$^{-1}$; the listed values are anharmonic vibrational wavenumbers predicted with the B3PW91/6-311++g(2*d*, 2*p*) method.

A C4–C$\ell$ bond length of 1.867 Å for *trans*-1-chloromethylallyl radical (**1a**) is predicted with the B3LYP/6-311++g(2*d*,2*p*) method, 0.028 Å greater than that predicted with the B3PW91/6-311++g(2*d*,2*p*) method, resulting to discrepancies in predicted harmonic/anharmonic vibrational wavenumbers of the CC$\ell$ stretching ($\nu_{21}$) mode of 592/569 cm$^{-1}$ for B3LYP and 636/610 cm$^{-1}$ for B3PW91. As will be discussed in Sec. V B, observed experimental value for this mode is 650.3 cm$^{-1}$, supporting the adequacy of using the B3PW91 method.

The predicted harmonic and anharmonic vibrational wavenumbers and IR intensities of 2-chloro-3-buten-1-yl ((**2a**) and (**2b**)) and 1-chloro-1-methylallyl (**3**) radicals are listed in Table SI of the supplementary material.[49] Lines of 2-chloro-3-buten-1-yl (**2a**) predicted for $\nu_{22}$ (404 cm$^{-1}$), $\nu_{20}$ (653 cm$^{-1}$), $\nu_{19}$ (708 cm$^{-1}$), and $\nu_{17}$ (947 cm$^{-1}$) have IR intensities greater than 30 km mol$^{-1}$ and those of 2-chloro-3-buten-1-yl (**2b**) predicted for $\nu_{22}$ (452 cm$^{-1}$), $\nu_{20}$ (645 cm$^{-1}$), $\nu_{19}$ (688 cm$^{-1}$), $\nu_{18}$ (830 cm$^{-1}$), and $\nu_{17}$ (948 cm$^{-1}$) have IR intensities greater than 15 km mol$^{-1}$; the vibrational modes for these molecules are ordered by wavenumber. Those of *trans*-1-chloro-1-methylallyl (**3**) predicted for $\nu_{20}$ (618 cm$^{-1}$), $\nu_{19}$ (767 cm$^{-1}$), $\nu_{14}$ (1134 cm$^{-1}$), $\nu_{12}$ (1281 cm$^{-1}$), $\nu_{10}$ (1424 cm$^{-1}$), and $\nu_6$ (2900 cm$^{-1}$) have IR intensities greater than 19 km mol$^{-1}$. All listed values are anharmonic vibrational wavenumbers.

### C. Reaction products of H + $C_4H_6$

According to the calculations of Miller using the G3//B3LYP/6-31G(d) method, five structural isomers of the straight chain $C_4H_7$ radical are stable.[51] Among these, each of the four isomers 1-methylallyl, 3-buten-1-yl, 2-buten-2-yl, and 1-buten-2-yl has two conformers, *cis* and *trans*, according to the structure of the CCCC skeleton, whereas the 1-buten-1-yl radical has four conformers (*cc*, *ct*, *tc*, and *tt*) because the terminal CCCH chain also has either a *cis* or *trans* configuration. The most stable structural isomer is the 1-methylallyl radical, $\bullet(CH_2CHCH)CH_3$, rationalized as due to the delocalization of the unpaired electron, and the other four structural isomers have energy at least 67 kJ mol$^{-1}$ greater than that of *trans*-1-methylallyl, which is more stable than *cis*-1-methylallyl radical. The isomerization between various structural isomers of $C_4H_7$ is unlikely to occur because of large barriers.

The geometries of two most likely reaction products of H + *trans*-1,3-butadiene, 1-methylally and 3-buten-1-yl radicals, predicted with the B3PW91/6-311++g(2*d*, 2*p*) method are illustrated in Fig. 2; the atomic numbering is indicated. The 1-methylallyl radical, $\bullet(CH_2CHCH)CH_3$, has a planar CCCC skeletal geometry with the unpaired electron delocalized over C1,C2, and C3. Of the two isomers, *trans*-1-methylallyl (**4a**) is more stable than *cis*-1-methylallyl (**4b**) by ~4 kJ mol$^{-1}$. For isomer (**4a**), the C1–C2 and C2–C3 bond lengths are 1.379 and 1.382 Å, respectively, similar to those of the allyl radical (1.387 Å).[52] The H6 atom of the methyl group is located in the molecular plane to have $C_s$ symmetry. In contrast, 3-buten-1-yl ($\bullet CH_2CH_2CH{=}CH_2$) has no conjugated structure and the CCCC skeleton is non-planar. For *trans*-3-buten-1-yl (**5a**), the CCCC dihedral angle is 119.6° and the C4H$_2$ group, on which the unpaired electron is located, is rotated about 27° from the C2C3C4 plane. The

TABLE II. Comparison of observed vibrational wavenumbers (in $cm^{-1}$) and relative IR intensities of the *trans*-1-chloromethylallyl (**1a**) radical with those of *trans*-1-chloromethylallyl (conformers (**1a**) and (**1b**)) predicted with the B3PW91/6-311++g(2*d*, 2*p*) method.

| | | (**1b**) | | (**1a**) | | |
|---|---|---|---|---|---|---|
| Mode[a] | Description[a] | Harmonic | Anharmonic | Harmonic | Anharmonic | *p*-$H_2$ |
| $\nu_1$ | *a*-$\nu_{C1H2}$ | 3253 (13)[b] | 3109 | 3255 (8)[b] | 3111 | 3112.8 (18)[c] |
| $\nu_2$ | $\nu_{C3H}$ | 3142 (11) | 3015 | 3176 (14) | 3040 | |
| $\nu_3$ | *a*-$\nu_{C4H2}$ | 3088 (4) | 2932 | 3158 (1) | 3015 | |
| $\nu_4$ | *s*-$\nu_{C1H2}$ | 3154 (19) | 3060 | 3156 (3) | 3037 | |
| $\nu_5$ | $\nu_{C2H}$ | 3171 (3) | 3041 | 3141 (9) | 3010 | |
| $\nu_6$ | *s*-$\nu_{C4H2}$ | 3052 (30) | 2947 | 3099 (15) | 2973 | 2962.3 (19) |
| $\nu_7$ | $\delta_{S\ C1H2} + \delta_{CCH} + a\text{-}\nu_{C1C2C3}$ | 1527 (12) | 1459 | 1524 (3) | 1468 | 1473.7 (5) |
| $\nu_8$ | $\delta_{CCH} + \delta_{S\ C1H2} + \delta_{S\ C4H2}$ | 1504 (18) | 1470 | 1502 (5) | 1458 | |
| $\nu_9$ | $\delta_{S\ C4H2}$ | 1457 (19) | 1436 | 1478 (4) | 1440 | 1442.6 (4) |
| $\nu_{10}$ | $\delta_{CCH}$ | 1339 (18) | 1310 | 1356 (10) | 1326 | 1328.2 (8) |
| $\nu_{11}$ | *s*-$\nu_{C1C2C3}$ | 1284 (34) | 1252 | 1289 (2) | 1264 | |
| $\nu_{12}$ | $\omega_{C4H2}$ | 1298 (30) | 1266 | 1254 (37) | 1228 | 1240.6 (38) |
| $\nu_{13}$ | *a*-$\nu_{C1C2C3}$ | 1201 (3) | 1167 | 1210 (2) | 1189 | |
| $\nu_{14}$ | $\nu_{C3–C4} + t_{C4H2}$ | 1176 (2) | 1149 | 1183 (16) | 1157 | 1163.0 (20) |
| $\nu_{15}$ | $t_{C4H2} + \nu_{C3–C4}$ | 1065 (10) | 1052 | 1110 (2) | 1089 | |
| $\nu_{16}$ | oop $\delta_{CH}$ | 999 (45) | 982 | 995 (34) | 966 | 962.2 (34) |
| $\nu_{17}$ | $\rho_{C1H2}$ | 923 (15) | 907 | 961 (5) | 948 | 947.5 (9) |
| $\nu_{18}$ | $\rho_{C4H2}$ | 902 (4) | 888 | 877 (6) | 867 | 870.5 (3) |
| $\nu_{19}$ | $\omega_{C1H2}$ + oop $\delta_{C1C2C3}$ | 800 (100) | 796 | 833 (78) | 824 | 809.0 (100) |
| $\nu_{20}$ | oop $\delta_{C1C2C3} + \omega_{C1H2}$ | 708 (3) | 702 | 786 (3) | 773 | 764.7 (5) |
| $\nu_{21}$ | $\nu_{C–C\ell\ (35)}$ | 715.7 (43) | 697.1 | 635.8 (100) | 610.1 | 650.3 (37) |
| | $\nu_{C–C\ell\ (37)}$ | 712.8 | 694.3 | 632.5 | 606.6 | 646.7 |
| $\nu_{22}$ | $t_{C1H2}$ | 532 (12) | 527 | 550 (20) | 533 | |
| $\nu_{23}$ | ip($\delta_{C1C2C3} + \delta_{C2C3C4}$) | 586 (11) | 577 | 499 (5) | 501 | |
| $\nu_{24}$ | oop $\delta_{C2C3C4}$ | 172 (2) | 167 | 325 (15) | 320 | |
| $\nu_{25}$ | op($\delta_{C1C2C3} + \delta_{C2C3C4}$) | 342 (1) | 341 | 278 (1) | 280 | |
| $\nu_{26}$ | $\tau_{C2–C3}$ | 63 (3) | 107 | 158 (4) | 151 | |
| $\nu_{27}$ | $\tau_{C3–C4}$ | 197 (7) | 200 | 78 (1) | 73 | |

[a]Approximate mode description and mode order follow those of (**1a**). $\nu$: stretch, $\delta$: bend or deformation, $\delta_S$: scissor, $\omega$: wag, $\rho$: rock, $\tau$: torsion, *t*: twist, *a*: antisymmetric, *s*: symmetric, oop: out-of-plane, ip: in-phase, op: out-of-phase. Numbering of C atoms is according to Fig. 1.

[b]Numbers in parentheses are IR intensities normalized to the most intense line. The intensities are 52.4 ($\nu_{19}$) and 69.7 ($\nu_{21}$) km $mol^{-1}$ for conformers (**1b**) and (**1a**), respectively.

[c]Numbers in parentheses are integrated intensities normalized to the most intense one.

lengths of the C1=C2 and C2–C3 bonds are 1.327 and 1.501 Å, respectively. For *cis*-3-buten-1-yl (**5b**), the four carbon atoms are nearly coplanar, with a dihedral angle of 9.3°.

The predicted harmonic and anharmonic vibrational wavenumbers and IR intensities of *trans*-1-methylallyl (**4a**) and *cis*-1-methylallyl (**4b**) radicals are listed in Table III; the mode order and approximate descriptions follow those of (**4a**). Lines of *trans*-1-methylallyl (**4a**) for $\nu_{23}$ ($C1H_2$ wag, 786 $cm^{-1}$), $\nu_{22}$ (out-of-plane CH band, 954 $cm^{-1}$), $\nu_{19}$ ($C4H_2$ antisym. stretch, 2902 $cm^{-1}$), $\nu_9$ ($C4H_2$ scissor, 1427 $cm^{-1}$), $\nu_6$ ($CH_3$ sym. stretch, 2877 $cm^{-1}$), $\nu_3$ (C3H stretch, 3016 $cm^{-1}$), and $\nu_2$ ($C1H_2$ sym. stretch, 3033 $cm^{-1}$) are predicted to have IR intensities greater than 20 km $mol^{-1}$. Those of *cis*-1-methylallyl (**4b**) for $\nu_{24}$ (out-of-plane C3H bend, 677 $cm^{-1}$), $\nu_{23}$ (755 $cm^{-1}$), $\nu_{19}$ (2910 $cm^{-1}$), $\nu_9$ (1415 $cm^{-1}$), $\nu_6$ (2885 $cm^{-1}$), $\nu_3$ (3054 $cm^{-1}$), and $\nu_2$ (3040 $cm^{-1}$), are predicted to have IR intensities greater than 20 km $mol^{-1}$. All listed values are anharmonic vibrational wavenumbers predicted with the B3PW91/6-311++g(2*d*, 2*p*) method.

The predicted harmonic and anharmonic vibrational wavenumbers and IR intensities of 3-buten-1-yl radical are listed in Table SII of the supplementary material.[49] Lines of *trans*-3-buten-1-yl (**5a**) for $\nu_{23}$ (526 $cm^{-1}$), $\nu_{19}$ (932 $cm^{-1}$), $\nu_8$ (1662 $cm^{-1}$), $\nu_7$ (2831 $cm^{-1}$), $\nu_6$ (2866 $cm^{-1}$), and $\nu_3$ (3032 $cm^{-1}$), and those of *cis*-3-buten-1-yl (**5b**) for $\nu_{24}$ (524 $cm^{-1}$), $\nu_{23}$ (528 $cm^{-1}$), $\nu_{19}$ (925 $cm^{-1}$), $\nu_8$ (1657 $cm^{-1}$), $\nu_7$ (2792 $cm^{-1}$), $\nu_6$ (2880 $cm^{-1}$), and $\nu_5$ (2989 $cm^{-1}$) are predicted to have IR intensities greater than 15 km $mol^{-1}$; the listed values are anharmonic vibrational wavenumbers predicted with the B3PW91/6-311++g(2*d*, 2*p*) method.

## IV. EXPERIMENTAL RESULTS

### A. Complex of $C\ell_2$ and $C_4H_6$

A partial IR absorption spectrum of $C_4H_6$ in solid *p*-$H_2$ (1/1400) at 3.3 K is shown in Fig. 3(a). Intense lines

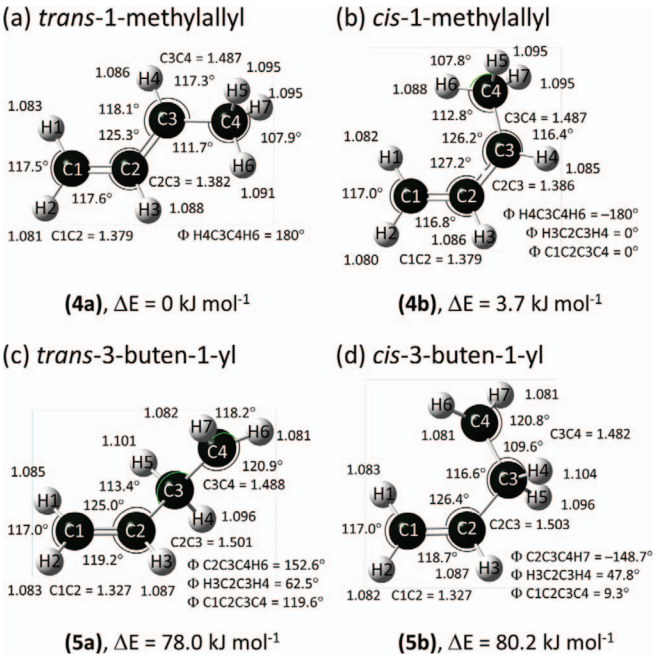


FIG. 2. Geometries of (a) *trans*-1-methylallyl (**4a**), (b) *cis*-1-methylallyl (**4b**), (c) *trans*-3-buten-1-yl (**5a**), and (d) *cis*-3-buten-1-yl (**5b**) predicted with the B3PW91/6-311++g(2*d*, 2*p*) method. Bond distances are in Å, and angles in degrees.

observed at 528.6, 907.9, 1015.2, 1378.9, and 1595.1 $cm^{-1}$, indicated with arrows in Fig. 3(a), agree with the literature values 524.5 ($\nu_{12}$), 908.1 ($\nu_{11}$), 1013.8 ($\nu_{10}$), 1380.8 ($\nu_{21}$), and 1596.4 $cm^{-1}$ ($\nu_{20}$) of gaseous *trans*-$C_4H_6$ (Ref. 53–55) and values 536, 925, 1030, 1383, and 1616 $cm^{-1}$ predicted quantum-chemically. Several lines in the region 2990−3100 $cm^{-1}$ were also observed; the fundamentals were observed at 2982.2, 3052.6, and 3098.5 $cm^{-1}$, tentatively assigned according to the literature values 3011 ($\nu_{19}$), 3035 (or 3054.7, $\nu_{18}$), and 3100.6 ($\nu_{17}$) $cm^{-1}$ of gaseous *trans*-$C_4H_6$.[53,54,56] Several lines at 1275.0, 1426.4, 1436.9, 1496.6, 1659.5, 2992.9, 3010.7, 3031.4/3030.3, and 3094.9 $cm^{-1}$, indicated with "o" in Fig. 3(a), are due to combination or overtone transitions. The weak lines, observed at 916.2 and 994.5/995.4 $cm^{-1}$ and indicated with *cis* in Fig. 3(a), are due to *cis*-1,3-butadiene (∼1.6%); corresponding lines were observed at 914 and 996 $cm^{-1}$ in a Ar matrix.[57] The difference spectrum of a $C\ell_2/C_4H_6/p$-$H_2$ (1.0/1.5/1500) matrix sample with lines of $C_4H_6$ stripped by subtraction of the scaled spectrum in Fig. 3(a) is shown in Fig. 3(b); some intense lines of $C_4H_6$ might have been stripped incompletely. The original intense lines of $C_4H_6$ listed above shifted to 534.2, 914.5, 1016.2, 1378.9, and 1591.8 $cm^{-1}$, and new features at 517.3/519.0, 524.4, 755.3, 918.9, 1281.8, and 1640.4 $cm^{-1}$ appeared. These lines are indicated as asterisks * in Fig. 3(b). These new features are assigned to absorption of the $C\ell_2$-$C_4H_6$ complex, to be discussed in Sec. V A. The observed wavenumbers and relative intensities are presented in Table I. The ratio of the $C\ell_2$-$C_4H_6$ complex to $C_4H_6$ is estimated to be approximately 1:10 according to observed integrated intensities of lines of $C_4H_6$ at 907.9 and 1595.1 $cm^{-1}$ and those of $C\ell_2$-$C_4H_6$ at 914.5 and 1591.8 $cm^{-1}$ and the corresponding IR intensities predicted with theory.

### B. Products of the reaction C$\ell$ + $C_4H_6$

Figure 4(a) shows the absorption spectrum of the $C_4H_6/C\ell_2/p$-$H_2$ (1/1.5/1500) matrix recorded after deposition. Figure 4(b) shows a difference spectrum after irradiation of the matrix at 365 nm for 1.5 h. The difference spectrum was obtained on subtracting the spectrum recorded in the preceding step from that recorded after this step; features pointing upward thus indicate production, whereas those pointing downward indicate destruction. Lines due to the $C\ell_2$-$C_4H_6$ complex decreased in intensity, those of $C_4H_6$ increased in intensity, and several new lines appeared; among them the most prominent ones are at 809.0, 962.2, and 1240.6 $cm^{-1}$. These lines and several weaker lines, showing similar relative intensities in disparate stages of various experiments, are indicated with arrows and wavenumbers in Fig. 4(b); a list is given in Table II. These lines are designated as group A and assigned to the *trans*-1-chloromethylallyl (**1a**) radical in Sec. V B. We estimated that about 40% of $C\ell_2$-$C_4H_6$ was reacted and ∼11% of $C_4H_6$ was reproduced according to the observed variation in line intensities.

After we continued irradiation at 365 nm for an additional 3 h, the difference spectrum is illustrated in Fig. 4(c). The intensities of lines in group A decreased, whereas those of several weak lines at 738.6/735.3, 933.6, 983.5, 1181.0, 1426.9, and 1447.9 $cm^{-1}$, indicated as * in Fig. 4(c), increased. These increasing weak features are readily assigned to 3,4-dichloro-1-butene, $H_2C{=}CHCHC\ell CH_2C\ell$, with assignments made according to the observed spectrum of 3,4-dichloro-1-butene isolated in $p$-$H_2$ recorded in a separate experiment. Weak lines at 967.8 and 1250.4 $cm^{-1}$, designated as # in Fig. 4(c), are tentatively assigned to 1,4-dichloro-2-butene according to the literature spectrum of gaseous 1,4-dichloro-2-butene.[58] These features became much more prominent when we employed a greater mixing ratio of $C\ell_2$, consistent with the expectation for dichloro compounds.

The intensities of lines of $C\ell_2$-$C_4H_6$ decreased continuously, those in group A increased in the initial stage, but diminished after further irradiation, whereas the intensities of lines of 3,4-dichloro-1-butene increased continuously. The integrated intensities of lines at 809.0 $cm^{-1}$ (group A, *trans*-1-chloromethylallyl), 738.9 $cm^{-1}$ (3,4-dichloro-2-butene), and 914.5 $cm^{-1}$ ($C\ell_2$-$C_4H_6$) are shown in Fig. S2 of the supplementary material.[49] In some experiments, the UV irradiated matrix was further irradiated for 1.5 h with light near 254 nm from a low-pressure Hg lamp. The intensities of lines in group A increased significantly, whereas those of 3,4-dichloro-1-butene decreased only slightly.

### C. Products of the reaction H + $C_4H_6$

Anderson and co-workers reported that C$\ell$ atoms might react with $p$-$H_2$ to form HC$\ell$ when the matrix is subjected to IR irradiation during acquisition of IR absorption spectra.[39,40] Utilizing the reaction C$\ell$ + $H_2$ → HC$\ell$ + H is thus an

TABLE III. Comparison of observed vibrational wavenumbers (in $cm^{-1}$) and IR intensities of the *trans*-1-methylallyl (**4a**) radical with those of *cis*-1-methylallyl (**4b**) and *trans*-1-methylallyl (**4a**) radicals predicted with the B3PW91/6-311++g(2*d*, 2*p*) method.

| | | | *cis*-1-methylallyl (**4b**) | | *trans*-1-methylallyl (**4a**) | | |
|---|---|---|---|---|---|---|---|
| Mode | Sym | Description[a] | Harmonic | Anharmonic | Harmonic | Anharmonic | *p*-$H_2$[b] |
| $\nu_1$ | a′ | *a*-$\nu_{C1H2}$ | 3253 (27)[c] | 3103 | 3250 (18)[c] | 3105 | 3107.3 (26)[d] |
| $\nu_2$ | a′ | *s*-$\nu_{C1H2}$ + $\nu_{C3H}$ | 3171 (44) | 3040 | 3153 (34) | 3033 | |
| $\nu_3$ | a′ | $\nu_{C3H}$ + *s*-$\nu_{C1H2}$ | 3162 (42) | 3054 | 3149 (36) | 3016 | 3023.5 (45) |
| $\nu_4$ | a′ | $\nu_{C2H}$ | 3143 (16) | 3010 | 3129 (12) | 3029 | |
| $\nu_5$ | a′ | $\nu_{C4H}$ | 3129 (17) | 2970 | 3109 (22) | 2964 | 2968.8 (28) |
| $\nu_6$ | a′ | *s*-$\nu_{CH3}$ | 3022 (62) | 2885 | 3013 (58) | 2877 | 2851.3 (19) |
| $\nu_7$ | a′ | $\delta_{CCH}$ + *a*-$\nu_{C1C2C3}$ | 1527 (12) | 1461 | 1529 (4) | 1501 | 1499.2 (3) |
| $\nu_8$ | a′ | $\delta_{S\ C1H2}$ | 1516 (12) | 1452 | 1509 (14) | 1467 | 1466.1 (9) |
| $\nu_9$ | a′ | $\delta_{S\ C4H2}$ | 1456 (47) | 1415 | 1472 (33) | 1427 | 1433.6 (42) |
| $\nu_{10}$ | a′ | $u_{CH3}$ | 1394 (6) | 1360 | 1405 (3) | 1375 | |
| $\nu_{11}$ | a′ | $\delta_{CCH}$ | 1434 (15) | 1396 | 1341 (2) | 1314 | 1304.4 (2) |
| $\nu_{12}$ | a′ | *s*-$\nu_{C1C2C3}$ | 1242 (1) | 1220 | 1286 (4) | 1257 | 1257.8 (4) |
| $\nu_{13}$ | a′ | *a*-$\nu_{C1C2C3}$ | 1202 (1) | 1174 | 1206 (1) | 1186 | 1186.0 (0) |
| $\nu_{14}$ | a′ | $\nu_{C3C4}$ + $\delta_{C1C2C3}$ | 1084 (15) | 1066 | 1144 (2) | 1120 | 1122.1 (1) |
| $\nu_{15}$ | a′ | $\rho_{C1H2}$ + $\omega_{C4H2}$ | 1022 (1) | 996 | 990 (10) | 979 | 978.6 (7) |
| $\nu_{16}$ | a′ | $\omega_{C4H2}$ + $\rho_{C1H2}$ | 881 (21) | 869 | 883 (12) | 876 | 879.0 (2) |
| $\nu_{17}$ | a′ | ip($\delta_{C1C2C3}$ + $\delta_{C2C3C4}$) | 572 (2) | 564 | 504 (1) | 507 | |
| $\nu_{18}$ | a′ | op($\delta_{C1C2C3}$ + $\delta_{C2C3C4}$) | 287 (1) | 265 | 283 (0) | 290 | |
| $\nu_{19}$ | a″ | *a*-$\nu_{C4H2}$ | 3061 (40) | 2910 | 3052 (31) | 2902 | 2917.1(15)/ 2922.2 (15) |
| $\nu_{20}$ | a″ | $t_{C4H2}$ | 1472 (17) | 1435 | 1469 (13) | 1427 | 1446.2 (13) |
| $\nu_{21}$ | a″ | $\rho_{C4H2}$ | 1020 (5) | 997 | 1024 (5) | 998 | 1006.5 (2) |
| $\nu_{22}$ | a″ | oop $\delta_{CH}$ | 986 (19) | 966 | 988 (49) | 954 | 957.9 (63) |
| $\nu_{23}$ | a″ | $\omega_{C1H2}$ + oop $\delta_{C3H}$ | 789 (100) | 755 | 794 (100) | 786 | 781.6 (100) |
| $\nu_{24}$ | a″ | oop $\delta_{C3H}$ + $\omega_{C1H2}$ | 698 (74) | 677 | 740 (0) | 720 | |
| $\nu_{25}$ | a″ | $t_{C1H2}$ | 534 (34) | 521 | 540 (13) | 525 | 525.1 (15) |
| $\nu_{26}$ | a″ | $\tau_{C2-C3}$ | 295 (2) | 289 | 217 (3) | 207 | |
| $\nu_{27}$ | a″ | $\tau_{C3-C4}$ | 60 (1) | 86 | 151 (2) | 114 | |

[a]Approximate mode description and mode order follow those of (**4a**). $\nu$: stretch, $\delta$: bend or deformation, $\delta_S$: scissor, $u$: umbrella, $\omega$: wag, $\rho$: rock, $\tau$: torsion, $t$: twist, *a*: antisymmetric, *s*: ymmetric, oop: out-of-plane, ip: in-phase, op: out-of-phase.
[b]Raman lines at 1904 ($2\nu_{22}$),1492 ($\nu_7$), 1265 ($\nu_{12}$), 872 ($\nu_{16}$), 499 ($\nu_{17}$), 289 ($\nu_{18}$), and 205 ($2\nu_{27}$) $cm^{-1}$ for the gaseous species were reported.[62]
[c]Numbers in parentheses are IR intensities normalized to the most intense line. The intensities are 38.3 ($\nu_{23}$) and 53.4 ($\nu_{23}$) km $mol^{-1}$ for conformers (**4b**) and (**4a**), respectively.
[d]Numbers in parentheses are integrated intensities normalized to the most intense one.

excellent method to produce H atoms in solid *p*-$H_2$. We have employed this method to investigate reactions of H + $C_2H_4$/•$CH_2CH_2C\ell$ (Ref. 59) and H + •$CHC\ell CH_3$.[60]

To promote the reaction of C$\ell$ atoms with *p*-$H_2$ matrix, we removed the 2.4-$\mu$m filter and increased the aperture to 10 mm to utilize more light from the IR source of the FTIR spectrometer to excite the UV-irradiated matrix. Figure 4(d) shows the difference spectrum after irradiation of the UV-irradiated matrix with IR light for 1 h. In addition to the much enhanced line of HC$\ell$ at 2894.1 $cm^{-1}$ and several weak ones of $(HC\ell)_n$ complexes in the region 2750−2900 $cm^{-1}$, several new lines appeared; they are distinct from those observed in group A shown in Fig. 4(b) and those of 3,4-dichloro-1-butene indicated as * in Fig. 4(c). Prominent features were observed at 781.6, 957.9, 1433.6, 3023.5, and 3107.1 $cm^{-1}$. These lines and several weaker lines showing similar relative intensities in various experiments, designated as group B and indicated with arrows and wavenumbers in Fig. 4(d), are assigned to the *trans*-1-methylallyl radical in Sec. V C. A list of observed lines is given in Table III. Other weak lines observed at 966.5, 1381.2, 1443.7, 1456.7, 2971.8, and 2944.8 $cm^{-1}$, marked with ∇ symbols in Fig. 4(d), likely correspond to *trans*-but-2-ene ($C_4H_8$),[61] even though we could not positively eliminate the possibility of a small contributions from *trans*-but-1-ene.

## V. DISCUSSION

### A. Assignments of the C$\ell_2$-$C_4H_6$ complex

New features observed in the C$\ell_2$/$C_4H_6$/*p*-$H_2$ matrix as compared with lines of $C_4H_6$ are indicated with * in Fig. 3(b). The stick spectra of $C_4H_6$ and C$\ell_2$-$C_4H_6$ according to predicted anharmonic vibrational wavenumbers and IR intensities are shown in Figs. 3(c) and 3(d), respectively. The observed features are listed in Table I and compared with theoretical predictions for C$\ell_2$-$C_4H_6$. The observed and predicted spectral shifts of C$\ell_2$-$C_4H_6$ from features of $C_4H_6$, also listed in Table I, agree each other satisfactorily. For instance, lines at 534.2 and 914.5 $cm^{-1}$ of C$\ell_2$-$C_4H_6$ are blueshifted from those

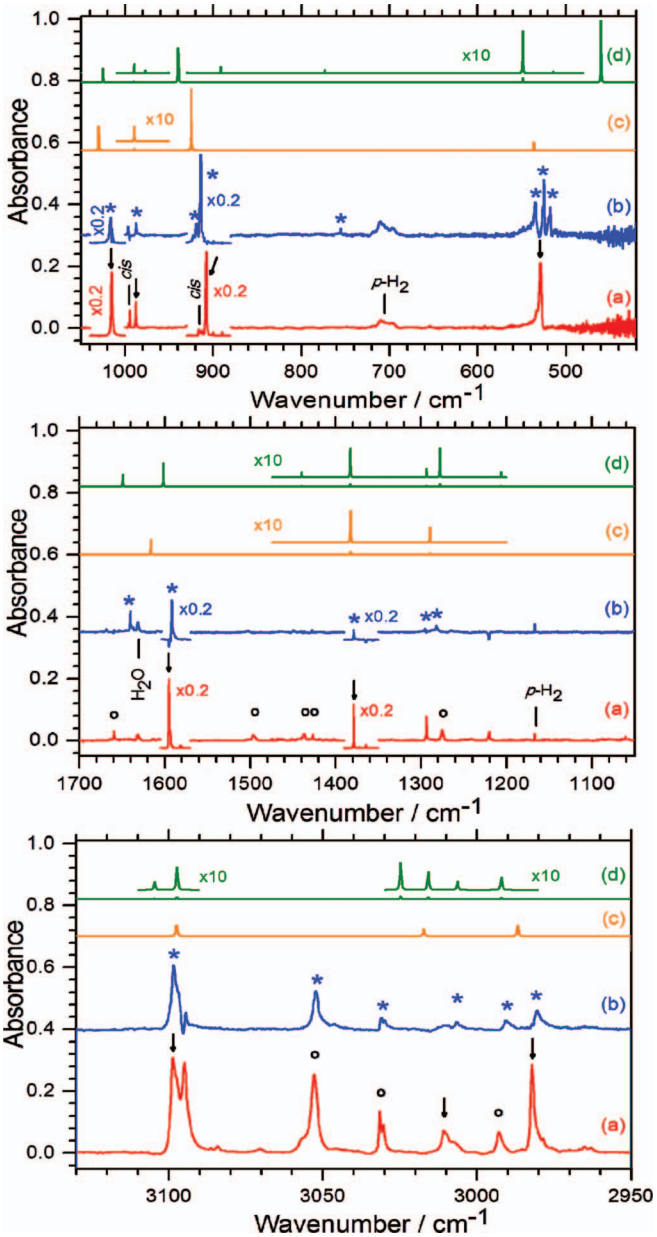


FIG. 3. (a) Absortion spectrum of a $C_4H_6/p$-$H_2$ (1/1400) matrix deposited at 3.3 K for 5 h. Fundamental lines are indicated with arrows and overtones or combination lines are indicated with o. (b) Absorption spectra of a $C\ell_2/C_4H_6/p$-$H_2$ (1/1.5/1500) matrix, deposited for 5 h and annealed at 4.3 K for 0.5 h, with lines of $C_4H_6$ stripped by subtraction of the scaled spectrum in (a); lines of $C\ell_2$-$C_4H_6$ are indicated with *. Both spectra were recorded at resolution of 0.25 cm$^{-1}$. (c) IR stick spectrum simulated according to anharmonic vibrational wavenumbers and IR intensities of $C_4H_6$ predicted with the B3PW91/6-311++g(2*d*, 2*p*) method. (d) simulated stick spectrum of $C\ell_2$-$C_4H_6$. Some intense lines were decreased and shifted downward for viewing convenience.

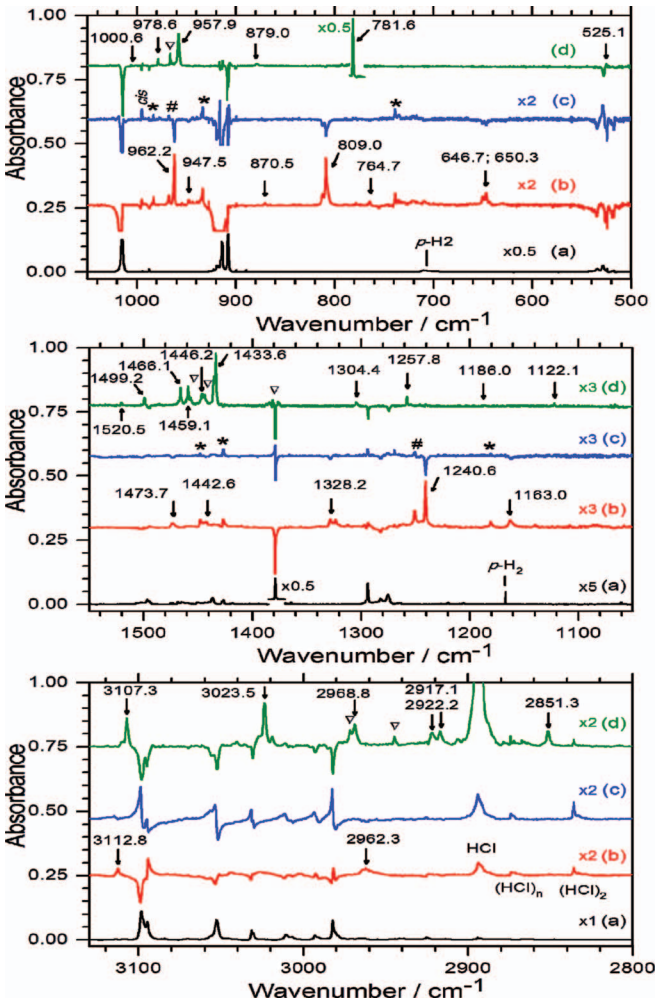


FIG. 4. (a) Absorption spectra of a $C\ell_2/C_4H_6/p$-$H_2$ (1/1.5/1500) matrix, deposited for 5 h and annealed at 4.3 K for 0.5 h. (b) Difference spectrum of the matrix after irradiation with light at 365 nm for 1.5 h. Lines in group A (*trans*-1-chloromethylallyl) are indicated with arrows and wavenumbers. (c) Difference spectrum of the matrix after further irradiation at 365 nm for additional 3 h. Lines of $C\ell_2C_4H_6$ are marked with * (3,4-dichloro-1-butene) and # (1,4-dichloro-2-butene). (d) Difference spectrum of the matrix after further irradiation with IR light for 1 h. Lines in group B (*trans*-1-methylallyl) are marked with arrows and and wavenumbers. The intense line at 781.6 cm$^{-1}$ is halved and shifted downward for viewing convenience. Lines marked with ∇ likely correspond to *trans*-but-2-ene ($C_4H_8$). All spectra were recorded at resolution 0.25 cm$^{-1}$.

of $C_4H_6$, whereas that at 1591.8 cm$^{-1}$ is redshifted. Formation of the $C\ell_2$-$C_4H_6$ complex lowers the symmetry of $C_4H_6$ so as to activate the originally IR inactive *gerade* modes ($a_g$, $b_g$) in the $C_{2h}$ symmetry. The new features observed at 755.3, 918.9, 1281.8, and 1640.4 cm$^{-1}$, shown in Fig. 3(b), correspond to the IR inactive modes of $\nu_{16}$ ($CH_2$ twist, $b_g$), $\nu_{15}$ ($CH_2$ wag, $b_g$), $\nu_6$ (CCH bend, $a_g$), and $\nu_4$ (C=C stretch, $a_g$) of $C_4H_6$, respectively. We hence assigned these new features marked with * in Fig. 3(b) to absorption of $C\ell_2$-$C_4H_6$.

Lines at 524.4 and 519.0/517.3 cm$^{-1}$ are assigned to the $C\ell C\ell$ stretching mode of $^{35}C\ell_2$-$C_4H_6$ and $^{35}C\ell^{37}C\ell$-$C_4H_6$/$^{37}C\ell^{35}C\ell$-$C_4H_6$, respectively. Observed isotopic shifts of −5.4 and −7.1 cm$^{-1}$ are consistent with theoretical predictions of −5.5 and −6.7 cm$^{-1}$, respectively. An extremely weak line at 510.3 cm$^{-1}$ might be assigned to $^{37}C\ell_2$-$C_4H_6$ with an observed shift of −14.1 cm$^{-1}$ near a predicted value of −12.3 cm$^{-1}$, but the poor signal-to-noise ratio precludes a definitive assignment. The observed intensity ratios of ∼9: 3: 4 for these lines are also consistent with the natural abundance of $^{35}C\ell$ : $^{37}C\ell \cong$ 3:1. This mode was predicted to have an anharmonic wavenumber of 460 cm$^{-1}$, much smaller than our observation. A similar trend was also observed for $C\ell_2$-$C_2H_4$; the $^{35}C\ell^{35}C\ell$ stretching mode was observed at 531.2 cm$^{-1}$, whereas the MP2/aug-cc-pVDZ method predicts

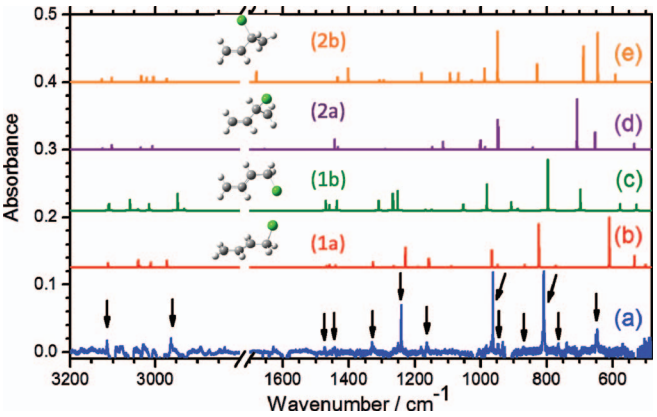


FIG. 5. (a) Difference spectra of a $C\ell_2/C_4H_6/p\text{-}H_2$ (1/1.5/1500) matrix after irradiation with light at 365 nm for 0.5 h. Lines in group A (*trans*-1-chloromethylallyl) are marked with arrows. IR stick spectra simulated according to anharmonic vibrational wavenumbers and IR intensities predicted with the B3PW91/6-311++g(2*d*, 2*p*) method are shown for (b) *trans*-1-chloromethylallyl (**1a**), (c) *trans*-1-chloromethylallyl (**1b**), (d) 2-chloro-3-buten-1-yl (**2a**), and (e) 2-chloro-3-buten-1-yl (**2b**).

471 cm$^{-1}$.[59] The discrepancy between observed and predicted vibrational wavenumbers might indicate that the interaction between $C\ell_2$ and $C_4H_6$ was overestimated by theory. The vibrational wavenumber of $C\ell_2$ is about 554 cm$^{-1}$.

In the C–H stretching region, lines at 3098.2, 3052.2, 3029.9, 3006.7, 2990.5, and 2980.4 cm$^{-1}$ were observed. The pattern follows that of $C_4H_6$, but we hesitate to provide definitive mode assignments except for the line at 3098.2 cm$^{-1}$ ($\nu_{17}$) because of the complication due to the presence of combination and overtone bands.

### B. Assignment of lines in group A to *trans*-1-chloromethylallyl (1a)

Upon photolysis of the $C_4H_6/C\ell_2/p\text{-}H_2$ matrix at 365 nm, we observed new IR lines in group A, indicated with arrows and wavenumbers in Fig. 4(b), and several weak lines of 3,4-dichloro-1-butene, indicated with * in Fig. 4(c). A spectrum recorded at an early stage of photolysis at 365 nm showing negligible contribution of 3,4-dichloro-1-butene is reproduced in Fig. 5(a). We expect that these features are due to the product of the reaction $C\ell + C_4H_6$. The stick IR spectra of possible products *trans*-1-chloromethylallyl ((**1a**) and (**1b**)) and 2-chloro-3-buten-1-yl ((**2a**) and (**2b**)) simulated according to anharmonic vibrational wavenumbers and IR intensities predicted with the B3PW91/6-311++g(2*d*, 2*p*) method are shown in Figs. 5(b)–5(e) for comparison.

The best agreement between experiment and theory in both wavenumbers and relative intensities is clearly with the spectrum predicted for *trans*-1-chloromethylallyl (**1a**) shown in Fig. 5(b). The observed wavenumbers and relative intensities are compared with theoretical predictions for (**1a**) and (**1b**) in Table II. Observed intense lines at 650.3, 809.0, 962.2, and 1240.6 cm$^{-1}$ agree satisfactorily with the calculated anharmonic vibrational wavenumbers and relative IR intensities for $\nu_{21}$ (CC$\ell$ stretch, 610 cm$^{-1}$), $\nu_{19}$ (C1H$_2$ wag, 824 cm$^{-1}$), $\nu_{16}$ (out-of-plane CH bend, 966 cm$^{-1}$), and $\nu_{12}$ (C4H$_2$ wag, 1228 cm$^{-1}$). A weaker line near 646.7 cm$^{-1}$ might be assigned to the CC$\ell$ stretching ($\nu_{21}$) mode of $\bullet(CH_2CHCH)CH_2{}^{37}C\ell$; the observed $^{37}C\ell$ isotopic shift of $-3.6$ cm$^{-1}$ is consistent with values $-3.3$ and $-3.5$ cm$^{-1}$ derived from predicted harmonic and anharmonic vibrational wavenumbers for configuration (**1a**). In the CH stretching region, weaker lines observed at 2962.3 and 3112.8 cm$^{-1}$ are assigned to the $\nu_6$ (C4H$_2$ sym. stretch, 2973 cm$^{-1}$) and $\nu_1$ (C1H$_2$ antisym. stretch, 3111 cm$^{-1}$) modes; other modes in this region suffer from interference due to absorption of the parent. The deviations between experiments and calculations are less than 15 cm$^{-1}$ (1.8%) except for $\nu_{21}$ (CC$\ell$ stretch) for which predicted harmonic and anharmonic vibrational wavenumbers are 636 and 610 cm$^{-1}$, respectively, but the observed line is at 646.7 cm$^{-1}$; the observed IR intensity is also smaller than predicted.

Although the other conformer *trans*-1-chloromethylallyl (**1b**) has a similar allyl structure, its predicted IR spectrum (Fig. 5(c)) differs distinctively from that of *trans*-1-chloromethylallyl (**1a**) and matches much less satisfactorily the observed spectrum in both wavenumbers and relative intensities. Similarly, the spectra of the two conformers of 2-chloro-3-buten-1-yl shown in Figs. 5(d) and 5(e) do not match the observed spectrum. The predicted vibrational wavenumbers and relative IR intensities of 1-chloro-1-methylallyl (not shown) also agree poorly with the observed lines in group A. Furthermore, it is unlikely that this species can be formed from a direct reaction of C$\ell$ with $C_4H_6$. We exclude also the *cis*-1-chloromethylallyl from our assignments because the barrier height for *trans-cis* isomerization is large and the predicted spectral pattern matches poorly with our observation. Hence, we assign the observed features in group A to *trans*-1-chloromethylallyl.

### C. Assignment of lines in group B to *trans*-1-methylallyl

As shown in Fig. 4(d), lines in group B appeared upon further irradiation of the UV-irradiated $C_4H_6/C\ell_2/p\text{-}H_2$ matrix with IR light from the spectrometer. We reproduce this trace in Fig. 6(a) and indicate lines in group B with arrows to compare with stick spectra, shown in Figs. 6(b)–6(e), of possible products *trans*-1-methylallyl (**4a**), *cis*-1-methylallyl (**4b**), *trans*-3-buten-1-yl (**5a**), and *cis*-3-buten-1-yl (**5b**) simulated according to anharmonic vibrational wavenumbers and IR intensities predicted with the B3PW91/6-311++g(2*d*, 2*p*) method. Lines marked with symbols ∇ likely correspond to *trans*-but-2-ene ($C_4H_8$).[61] The best agreement in both wavenumbers and relative intensities is clearly with the spectrum predicted for *trans*-1-methylallyl (**4a**) shown in Fig. 6(b). The observed wavenumbers and relative intensities are compared with theoretical predictions for (**4a**) and (**4b**) in Table III.

The intense lines observed at 781.6, 957.9, 1433.6, 2968.8, 3023.5, and 3107.3 cm$^{-1}$ agree with anharmonic vibrational wavenumbers predicted for the $\nu_{23}$ (C1H$_2$ wag, 786 cm$^{-1}$), $\nu_{22}$ (out-of-plane CH bend, 954 cm$^{-1}$), $\nu_9$ (C4H$_2$ scissor, 1427 cm$^{-1}$), $\nu_5$ (C4H stretch, 2964 cm$^{-1}$), $\nu_3$ (CH$_2$ sym. stretch, 3016 cm$^{-1}$) or $\nu_2$ (C1H$_2$ sym. stretch, 3033 cm$^{-1}$), and $\nu_1$ (C1H$_2$ antisym. stretch, 3105 cm$^{-1}$)

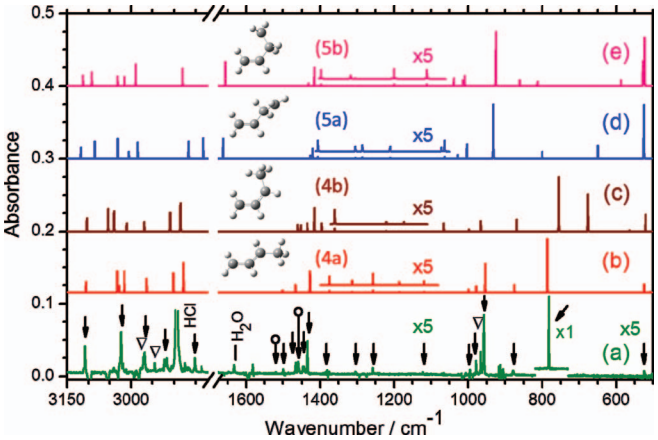


FIG. 6. (a) Difference spectra of a $C\ell_2/C_4H_6/p\text{-}H_2$ (1/1.5/1500) matrix irradiated at 365 nm after further irradiation with IR light for 1 h. Lines in group B are indicated with arrows and overtones or combination lines are indicated with o. Lines marked with ∇ likely correspond to *trans*-but-2-ene ($C_4H_8$). IR stick spectra simulated according to anharmonic vibrational wavenumbers and IR intensities predicted with the B3PW91/6-311++g(2*d*, 2*p*) method are shown for (b) *trans*-1-methylallyl (**4a**), (c) *cis*-1-methylallyl (**4b**), (d) *trans*-3-buten-1-yl (**5a**), and (e) *cis*-3-buten-1-yl (**5b**).

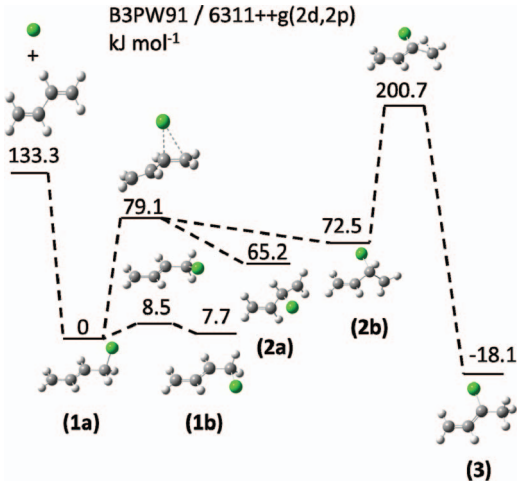


FIG. 7. Potential-energy diagram for the reactions of C$\ell$ + *trans*-1,3-butadiene to form 1-chloromethylallyl (**1a**), 1-chloromethylallyl (**1b**), 2-chloro-3-buten-1-yl (**2a**), 2-chloro-3-buten-1-yl (**2b**), and *trans*-1-chloro-1-methylallyl (**3a**). Energies predicted with the B3PW91/6-311++g(2*d*, 2*p*) method and corrected for the zero point energy are listed in kJ mol$^{-1}$.

modes of *trans*-1-methylallyl; some CH stretching lines could not be identified because of interference from the parent absorption. Lines at 1459.1 and 1520.5 cm$^{-1}$, indicated with symbols o in Fig. 6(a), might be due to combination or overtone transitions. The deviations between experiments and calculations are less than 10 cm$^{-1}$ except $\nu_6$ (25 cm$^{-1}$, 0.9%) and $\nu_{20}$ (−19 cm$^{-1}$, 1.3%). Several lines ($\nu_7$ at 1499.2, $\nu_{12}$ at 1257.8 and $\nu_{16}$ at 879.0 cm$^{-1}$) agree with those (1492, 1265, and 872 cm$^{-1}$) reported in the Raman spectrum of gaseous *trans*-1-methylallyl.[62]

Although the other conformer *cis*-1-methylallyl (**4b**) has a similar allyl structure, its predicted IR spectrum (Fig. 6(c)) differs significantly from that of *trans*-1-methylallyl (**4a**), especially in the region 600–1000 cm$^{-1}$, and matches poorly the observed spectrum in both wavenumbers and relative intensities. Similarly, as shown in Figs. 6(d) and 6(e), *trans*-3-buten-1-yl (**5a**) and *cis*-3-buten-1-yl (**5b**) are predicted to have spectral patterns significantly different from the observed spectrum. We hence conclude that the carrier of the observed new features in group B is *trans*-1-methylallyl.

### D. Reaction mechanism

Lines in group A are assigned to *trans*-1-chloromethylallyl (**1a**) and no spectral lines of 2-chloro-3-buten-1-yl were identified. We thus conclude that in a solid *p*-$H_2$ matrix, the C$\ell$ atom reacts selectively at the terminal carbon atom of *trans*-1,3-butadiene to generate the *trans*-1-chloromethylallyl radical rather than at the central carbon atom to form the 2-chloro-3-buten-1-yl radical.

To understand possible reaction paths, we performed DFT calculations using the B3PW91/6-311++g(2*d*, 2*p*) method. According to the energy diagram in Fig. 7, only one accessible entrance channel is identified, in which the reacting C$\ell$ atom attacks the terminal C atom of $C_4H_6$ to form 1-chloro-methylallyl with no barrier. We failed to identify a reaction channel for the C$\ell$ atom to attack directly the central C atom to form 2-chloro-3-buten-1-yl. The *trans*-1-chloromethylally radical (**1a**) is more stable by ∼65 kJ mol$^{-1}$ than 2-chloro-3-buten-1-yl (**2a**), and the barrier height for isomerization from (**1a**) to (**2a**) is ∼79 kJ mol$^{-1}$. Although the energy of this barrier is still smaller than that of the reactant C$\ell$ + $C_4H_6$, we expect rapid quenching of excess energy in solid *p*-$H_2$ after the addition reaction occurs, so the isomerization (**1a**) to (**2a**) unlikely occurs. Although *trans*-1-chloro-1-methylallyl (**3**) is more stable than *trans*-1-chloromethylallyl (**1a**) by ∼18 kJ mol$^{-1}$, we identified no direct reaction path from C$\ell$ + $C_4H_6$. Isomerization from 2-chloro-3-buten-1-yl (**2b**) to form *trans*-1-chloro-1-methylallyl (**3**) has a large barrier (∼128 kJ mol$^{-1}$). Our observation of only *trans*-1-chloromethylallyl (**1a**) agrees with the theoretical prediction.

The barrier to convert conformer (**1a**) of 1-chloromethylallyl to conformer (**1b**) was calculated to be ∼9 kJ mol$^{-1}$. The fact that we observed only *trans*-1-chloromethylallyl (**1a**), not conformer (**1b**), indicates that either the internal rotation of the chloromethyl moiety around the C3–C4 bond is hindered in solid *p*-$H_2$ or the quenching is so rapid that conversion from (**1a**) to (**1b**) is infeasible. We previously reported that internal rotation of $CH_3OH$ persists in solid *p*-$H_2$,[38] but the large size of the chlorine atom and the geometry of *trans*-1-chloromethylallyl in solid *p*-$H_2$ might hinder the internal rotation.

The intensities of lines of 3,4-dichloro-1-butene increased continuously with period of irradiation at 365-nm, and also as the mixing ratio of $C\ell_2$ was increased. At the later period of irradiation, the rate of growth of $C\ell_2C_4H_6$ is nearly equal to the rate of decrease of $C\ell C_4H_6$, as shown in Fig. S2 of the supplementary material,[49] indicating that the secondary reaction of a chlorine atom with $C\ell C_4H_6$ produces $C\ell_2C_4H_6$. The observation that the second chlorine atom attaches to the C1 and C3 positions of *trans*-1-chloromethylallyl (**1a**) is consistent with a radical center delocalized among C1, C2, and

C3. That observed lines of 3,4-dichloro-1-butene are more intense than those of 1,4-dichloro-2-butene might indicate that the secondary addition of chlorine to the carbon (C3) adjacent to the chloromethyl moiety of *trans*-1-chloromethylallyl (**1a**) is favored if both C$\ell$ atoms are from the same C$\ell_2$.

Lines in group B are assigned to absorption of *trans*-1-methylallyl (**4a**); no spectral lines of *trans*-3-buten-1-yl (**5a**) are identified. We thus conclude that in a solid *p*-$H_2$ matrix, the addition of the H atom occurs at the terminal carbon of *trans*-1,3-butadiene to yield *trans*-1-methylallyl rather than at the central carbon to yield 3-buten-1-yl. A theoretical calculation reported by Miller predicted the same behavior.[51] The reaction channel of H + *trans*-1,3-butadiene to form *trans*-1-methylallyl (Fig. 4 of Ref. 51) is nearly barrierless, whereas the transition state for formation of 3-buten-1-yl has energy ~21 kJ $mol^{-1}$ greater than that of the reactants. The primary product *trans*-1-methylallyl radical is more stable than *trans*-3-buten-1-yl by ~67 kJ $mol^{-1}$, and the isomerization from (**4a**) to (**5a**) following migration of a hydrogen atom from the terminal carbon to the central carbon has a large barrier of 205 kJ $mol^{-1}$. Although the energy of *cis*-1-methylallyl is predicted to be greater than that of *trans*-1-methylallyl by only~4 kJ $mol^{-1}$, the barrier for *trans-cis* isomerization in the gaseous phase is predicted to be ~59 kJ $mol^{-1}$;[51] in the environment of a cold *p*-$H_2$ matrix, this isomerization is unlikely to occur. According to the calculations, formation of other isomers – 2-buten-2-yl, 1-buten-2-yl, and 1-buten-1-yl – cannot occur directly from H + $C_4H_6$; isomerization from 1-methylallyl or 3-buten-1-yl also encounters large barriers.[51] Our observation of *trans*-1-methylallyl as the major product is consistent with theoretical predictions.

### E. Comparison with the reaction C$\ell$ + $C_3H_6$ in the *p*-$H_2$ matrix

The present experiments clearly demonstrate that, for the reaction C$\ell$ + *trans*-1,3-butadiene in a *p*-$H_2$ matrix, the reacting C$\ell$ atom attacks selectively the terminal carbon atom of the C=C double bond to form the *trans*-1-chloromethylallyl radical, in agreement with theoretical predictions of the path of minimum energy. This result is in contrast to the reaction C$\ell$ + $C_3H_6$ in a *p*-$H_2$ matrix in which the reacting C$\ell$ atom attacks the central carbon atom of $C_3H_6$ so that 2-chloropropyl radical was observed as the major product.[36] In the gaseous phase the formation of 1-chloropropyl has been reported to be much favored over 2-chloropropyl.[37]

The size restriction and steric effects within the solid *p*-$H_2$ matrix were proposed to be responsible for this unique selectivity of the reaction C$\ell$ + $C_3H_6$ in *p*-$H_2$.[36] These authors performed DFT calculations in which the geometry of the C$\ell_2$-$C_3H_6$ complex was optimized within the *p*-$H_2$ lattice at the B3LYP/aug-cc-pVDZ level while holding the *p*-$H_2$ lattice fixed in space. At 3.2 K, solid *p*-$H_2$ has a hexagonally close-packed (hcp) crystal structure; within a single hcp layer each *p*-$H_2$ molecule is separated by 3.76 Å.[23] The constraints of the *p*-$H_2$ lattice produce substantial changes in the geometry of the C$\ell_2$-$C_3H_6$ complex. In the gaseous phase, the distances between the reacting chlorine atom (the one adjacent to the $C_3H_6$) and the terminal and central carbon atoms of $C_3H_6$ are predicted to be 2.822 Å and 2.925 Å, respectively, whereas in the *p*-$H_2$ lattice the corresponding distances were predicted to be 3.107 and 2.847 Å, respectively. The calculations thus indicate that in a *p*-$H_2$ lattice the reacting C$\ell$ atom will be much nearer the central carbon atom than the terminal carbon atom, as opposed to the gaseous phase in which the C$\ell$ atom is nearer the terminal carbon. Upon photolysis of C$\ell_2$, the *p*-$H_2$ lattice *guides* the C$\ell$ atom to the central carbon atom of $C_3H_6$, located in a single substitutional site of the *p*-$H_2$ lattice, through the steric effect.

To examine the C$\ell$ + $C_4H_6$ reaction in solid *p*-$H_2$, we performed a similar calculation for C$\ell_2$-$C_4H_6$ embedded in the *p*-$H_2$ lattice with the B3PW91/6-31++G(2*d*, 2*p*) method. As $C_4H_6$ is larger than $C_3H_6$, a double substitutional site is required to accommodate the $C_4H_6$ molecule. With an initial geometry of C$\ell_2$-$C_4H_6$ predicted in the gaseous phase, we placed the C$\ell_2$-$C_4H_6$ complex in the *p*-$H_2$ lattice such that the C=C double bonds of the C$\ell_2$-$C_4H_6$ complex is nearly parallel to the *bc* plane of the hcp lattice and C$\ell_2$ is nearly parallel to the *a* axis. The geometry of the C$\ell_2$-$C_4H_6$ complex was then optimized with the *p*-$H_2$ lattice fixed in space. The structure of C$\ell_2$-$C_4H_6$ resulted from this optimization is compared with that of gaseous C$\ell_2$-$C_4H_6$ in Fig. 8. The *p*-$H_2$ molecules are represented with single blue spheres and some *p*-$H_2$ molecules are removed to reveal the structure of C$\ell_2$-$C_4H_6$. At the same level of calculation, the distances between the reacting chlorine atom and the terminal and middle carbon atoms of $C_4H_6$ in gaseous C$\ell_2$-$C_4H_6$ are predicted to be 2.773 Å and 3.007 Å, respectively, whereas in the *p*-$H_2$ lattice the corresponding distances were predicted to be 2.697 and 3.040 Å, respectively; the reacting C$\ell$ atom moves toward the terminal carbon atom slightly in solid *p*-$H_2$. Because $C_4H_6$ is located in a double substitutional site, the steric effect of the *p*-$H_2$ lattice pushes the reacting chlorine atom toward the

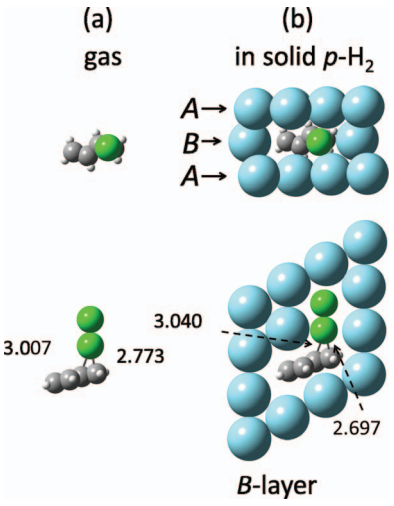


FIG. 8. Structures of the C$\ell_2$-$C_4H_6$ complex of minimum energy in the gaseous phase (a) and within a model hexagonal close-packed lattice of *p*-$H_2$ (b) calculated at the B3PW91/6-31++g(2*d*, 2*p*) level of theory. Top panels are views from the top of the complex looking down the C$\ell$–C$\ell$ axis and bottom panels are side views obtained by rotating the structures approximately 90° from those displayed in the top panel. The *p*-$H_2$ molecules are represented with single blue spheres and some *p*-$H_2$ molecules are removed to reveal the structure of C$\ell_2$-$C_4H_6$.

terminal carbon slightly as compared with gaseous $C\ell_2$-$C_4H_6$. The reaction $C\ell$ + *trans*-1,3-butadiene hence follows the path of minimum energy as predicted in the gaseous phase to form *trans*-1-chloromethylallyl radicals.

## VI. CONCLUSION

The reaction of $C\ell$ and H atoms with *trans*-1,3-butadiene in a *p*-$H_2$ matrix has been studied with IR spectroscopy. When the $C\ell_2/C_4H_6/p$-$H_2$ matrix was irradiated with UV light at 365 nm, a group of new lines with intense ones at 646.7, 809.0, 962.2, and 1240.6 $cm^{-1}$ are assigned to the *trans*-1-chloromethylallyl (**1a**) radical according to the expected reaction, the anharmonic vibrational wavenumbers and IR intensities predicted with the B3PW91/6-311++g(2*d*, 2*p*) method. We conclude that the addition of the $C\ell$ atom to $C_4H_6$ in the *p*-$H_2$ matrix occurs primarily at the terminal carbon atom, consistent with theoretical predictions but in contrast to the reaction of $C\ell$ + propene in which the addition of $C\ell$ to the central carbon atom is favored because of the steric effects in the *p*-$H_2$ matrix. These results demonstrate further that the cage effect of solid *p*-$H_2$ is diminished so that an isolated $C\ell$ atom can be produced via photodissociation of $C\ell_2$ *in situ*, and subsequently reacts with $C_4H_6$ to form the 1-chloromethylallyl radical.

When the UV-irradiated $C\ell_2/C_4H_6/p$-$H_2$ matrix was further irradiated with IR light from the spectrometer, a group of new lines with intense ones at 781.6, 957.9, 1433.6, 2851.3, 2968.8, and 3107.3 $cm^{-1}$ are assigned to the *trans*-1-methylallyl (**4a**) radical. The *trans*-1-methylallyl radical was produced because of the site-selective reaction of H atom with $C_4H_6$, as predicted with theory;[51] H atoms were produced from the reaction of $C\ell$ atom with IR-irradiated *p*-$H_2$ matrix.

## ACKNOWLEDGMENTS

National Science Council (NSC) (Grant No. NSC100-2745-M-009-001-ASP) and Ministry of Education of Taiwan ("Aim for Top University Plan" of National Chiao Tung University) supported this work. The National Center for High-Performance Computing provided computer time. K. Tanaka thanks NSC for the visiting professorship in National Chiao Tung University.

[1] S. G. Davis, C. K. Law, and H. Wang, J. Phys. Chem. A **103**, 5889 (1999).
[2] A. Laskin, H. Wang, and C. K. Law, Int. J. Chem. Kinet. **32**, 589 (2000).
[3] J. M. Roscoe, I. S. Jayaweera, A. L. Mackenzie, and P. D. Pacey, Int. J. Chem. Kinet. **28**, 181 (1996).
[4] J. M. Roscoe, A. R. Bossard, M. H. Back, and P. D. Pacey, Can. J. Chem. **78**, 16 (2000).
[5] J. A. Mueller, B. F. Parsons, L. J. Butler, F. Qi, O. Sorkhabi, and A. G. Suits, J. Chem. Phys. **114**, 4505 (2001).
[6] J. L. Miller, M. L. Morton, L. J. Butler, F. Qi, M. J. Krisch, and J. Shu, J. Phys. Chem. A **106**, 10965 (2002).
[7] D. E. Szpunar, Y. Liu, M. J. McCullagh, L. J. Butler, and J. Shu, J. Chem. Phys. **119**, 5078 (2003).
[8] M. L. Morton, L. J. Butler, T. A. Stephenson, and F. Qi, J. Chem. Phys. **116**, 2763 (2002).
[9] M. J. S. Dewar and S. Olivella, J. Am. Chem. Soc. **101**, 4958 (1979).
[10] X.-M. Zhang, J. Org. Chem. **63**, 1872 (1998).
[11] R. Gomez-Balderas, M. L. Coote, D. J. Henry, H. Fischer, and L. Radom, J. Phys. Chem. A **107**, 6082 (2003).
[12] P. George, J. P. Glusker, and C. W. Bock, J. Phys. Chem. A **104**, 11347 (2000).
[13] S. M. Clegg, B. F. Parsons, S. J. Klippenstein, and D. L. Osborn, J. Chem. Phys. **119**, 7222 (2003).
[14] I. Fisher and P. Chen, J. Phys. Chem. A **106**, 4291 (2002).
[15] C. L. Parker and A. L. Cooksy, J. Phys. Chem. A **103**, 2160 (1999).
[16] T. L. Nguyen, A. M. Mebel, and R. I. Kaiser, J. Phys. Chem. A **107**, 2990 (2003).
[17] H.-Y. Lee, V. V. Kislov, S.-H. Lin, A. M. Mebel, and D. M. Neumark, Chem. Eur. J. **9**, 726 (2003).
[18] B. J. Finlayson-Pitts and J. N. Pitts, Jr., *Chemistry of the Upper and Lower Atmosphere—Theory, Experiments, and Applications* (Academic, San Diego, CA, 2000).
[19] A. D. Kiel and P. B. Shepson, J. Geophys. Res., [Atmos.] **111**, D17303, doi:10.1029/2006JD007119 (2006).
[20] P. J. Tackett, A. E. Cavender, A. D. Kiel, P. B. Shepson, J. W. Bottenheim, S. Morin, J. Deary, A. Steffen, and C. Doerge, J. Geophys. Res. **112**, D07306, doi:10.1029/2006JD007785 (2007).
[21] P. Braña, B. Menendez, T. Fernandez, and J. A. Sordo, J. Phys. Chem. A **104**, 10842 (2000).
[22] P. Braña and J. A. Sordo, J. Am. Chem. Soc. **123**, 10348 (2001).
[23] P. Braña and J. A. Sordo, J. Comput. Chem. **24**, 2044 (2003).
[24] C. A. Taatjes, Int. Rev. Phys. Chem. **18**, 419 (1999).
[25] M. L. Poutsma, Science **157**, 997 (1967).
[26] F. Freeman, Chem. Rev. **75**, 439 (1975).
[27] T. Momose and T. Shida, Bull. Chem. Soc. Jpn. **71**, 1 (1998).
[28] T. Yoshioka, P. L. Raston, and D. T. Anderson, Int. Rev. Phys. Chem. **25**, 469 (2006).
[29] J. van Krandendonk, *Solid Hydrogen: Theory of the Properties of Solid $H_2$, HD, and $D_2$* (Plenum, New York, 1983).
[30] J. Ceponkus, P. Uvdal, and B. Nelander, J. Phys. Chem. A **114**, 6829 (2010).
[31] P. L. Raston and D. T. Anderson, J. Chem. Phys. **126**, 021106 (2007).
[32] T. Momose, M. Miki, M. Uchida, T. Shimizu, I. Yoshizawa, and T. Shida, J. Chem. Phys. **103**, 1400 (1995).
[33] N. Sogoshi, T. Wakabayashi, T. Momose, and T. Shida, J. Phys. Chem. A **101**, 522 (1997).
[34] Y.-F. Lee and Y.-P. Lee, J. Chem. Phys. **134**, 124314 (2011).
[35] C.-W. Huang, Y.-C. Lee, and Y.-P. Lee, J. Chem. Phys. **132**, 164303 (2010).
[36] J. Amicangelo and Y.-P. Lee, J. Phys. Chem. Lett. **1**, 2956 (2010).
[37] F. S. C. Lee and F. S. Rowland, J. Phys. Chem. **81**, 1222 (1977).
[38] Y.-P. Lee, Y.-J. Wu, R. M. Lees, L.-H. Xu, and J. T. Hougen, Science **311**, 365 (2006).
[39] P. L. Raston and D. T. Anderson, Phys. Chem. Chem. Phys. **8**, 3124 (2006).
[40] S. C. Kettwich, P. L. Raston, and D. T. Anderson, J. Phys. Chem. A **113**, 7621 (2009).
[41] A. D. Becke, J. Chem. Phys. **98**, 5648 (1993).
[42] J. P. Perdew, J. A. Chevary, S. H. Vosko, K. A. Jackson, M. R. Pederson, D. J. Singh, and C. Fiolhais, Phys. Rev. B **46**, 6671 (1992).
[43] K. Burke, J. P. Perdew, and Y. Wang, in *Electronic Density Functional Theory: Recent Progress and New Directions*, edited by J. F. Dobson, G. Vignale, and M. P. Das (Plenum, New York, 1998).
[44] R. A. Kendall, T. H. Dunning, Jr., and R. J. Harrison, J. Chem. Phys. **96**, 6796 (1992).
[45] Y. Zhao and D. G. Truhlar, J. Phys. Chem. A **108**, 6908 (2004).
[46] Y. Zhao and D. G. Truhlar, J. Chem. Theory Comput. **2**, 1009 (2006).
[47] Y. Zhao and D. G. Truhlar, J. Chem. Theory Comput. **3**, 289 (2007).
[48] M. J. Frisch, G. W. Trucks, H. B. Schlegel *et al.*, GAUSSIAN 09, Revision A.02, Gaussian, Inc., Wallingford, CT, 2009.
[49] See supplementary material at http://dx.doi.org/10.1063/1.4745075 for geometries of *trans*-1,3-butadiene ($C_4H_6$) and $C\ell_2$-$C_4H_6$ complex, integrated line intensities of observed species as a function of the UV irradiation period, and vibrational wavenumbers and IR intensities of 2-chloro-3-buten-1-yl, 1-chloro-1-methylallyl, *trans*-3-buten-1-yl and *cis*-3-buten-1-yl radicals.
[50] N. C. Craig, P. Groner, and D. C. McKean, J. Phys. Chem. A **110**, 7461 (2006).
[51] J. L. Miller, J. Phys. Chem. A **108**, 2268 (2004).
[52] E. Hirota, C. Yamada, and M. Okunishi, J. Chem. Phys. **97**, 2963 (1992).
[53] N. C. Craig, J. L. Davis, K. A. Hanson, M. C. Moore, K. J. Weidenbaum, and M. Lock, J. Mol. Struct. **695-696**, 59 (2004).
[54] Y. N. Panchenko, J. V. Auwera, Y. Moussaoui, and G. R. De Maré, Struct. Chem. **14**, 337 (2003).
[55] K. B. Wiberg and R. E. Rosenberg, J. Am. Chem. Soc. **112**, 1509 (1990).

[56]M. Hanlonen, L. Hanolen, and D. J. Nesbitt, J. Phys. Chem. A **108**, 3367 (2004).
[57]B. R. Arnold, V. Balaji, and J. Michl, J. Am. Chem. Soc. **112**, 1808 (1990).
[58]Coblentz Society, Inc., "Evaluated infrared reference spectra" in *NIST Chemistry WebBook*, NIST Standard Reference Database Number 69, edited by P. J. Linstrom and W. G. Mallard (National Institute of Standards and Technology, Gaithersburg, MD, 1988), see http://webbook.nist.gov.
[59]J. C. Amicangelo, B. Golec, M. Bahou, and Y.-P. Lee, Phys. Chem. Chem. Phys. **14**, 1014 (2012).
[60]B. Golec and Y.-P. Lee, J. Chem. Phys. **135**, 174302 (2011).
[61]A. J. Barnes and J. D. R. Howells, J. Chem. Soc., Faraday Trans. 2 **69**, 532 (1973).
[62]D. H. Tarrant, J. D. Getty, X. Liu, and P. B. Kelly, J. Phys. Chem. **100**, 7772 (1996).